UDC 532.526: 533.697

TECHNICAL REPORT OF NATIONAL AEROSPACE LABORATORY

TR-278T

Development of Turbulent Boundary Layers Along the Curved Walls of an Annular Diffusing Passage

Shoichi FUJII and Theodore H. OKIISHI

February 1972

NATIONAL AEROSPACE LABORATORY

CHŌFU, TOKYO, JAPAN

List of NAL Technical Reports

TR-248	A Description of the Ideas Underlying a Computer Programme for Predicting the Aerofoil Pressure Distributions in Subcritical Viscous Flow	Masao EBIHARA, Youji ISHIDA & Tokio OKONOGI	Nov. 1971
TR-249	Modified Optimization Algorithm for Computer Storage Problems in Generalized Newton-Raphson Method	Toru SHIHO	Oct. 1971
TR-250	Large Deflection of Cantilever Beams	Yasuo TADA & KAZUO KUSAKA	Oct. 1971
TR-251	Inertial Force Fiele Due to Nutational Motion of Spinning Axisymmetric Satellite and Its Application to Nutation Damper	Chikara MURAKAMI & Yoshiaki OHKAMI	Nov. 1971
TR-252T	A Study of Subsonic Two-Dimensional Wall-Interference Effects in a Perforated Wind Tunnel with Particular Reference to the NAL 2m×2m Transonic Wind Tunnel Inapplicability of the Conventional Boundary Condition	Masao EBIHARA	Dec. 1971
TR-253	A Calculation of Profile Drag of Airfoils in Compressible Flow	Youji ISHIDA	Nov. 1971
TR-254	Interference Between Wing and Surface of Velocity Discontinuity	Norio INUMARU	Nov. 1971
TR-255	The Study on the Motion of an Artificial Satellite in the Earth's Gravitational Field	Sumio TAKEUCHI & Koichi MATSUSHIMA	Dec. 1971
TR-256	On the Aerodynamic Damping Moment in Pitch of a Rigid Helicopter Rotor in Hovering	Kingo TAKAZAWA	Nov. 1971
TR-257	The Dynamic Stability of a Connected Rod under Periodic Longitudinal Force	Masaaki SANO	Jan. 1972
TR-258	Three Dimensional Suboptimal Explicit Guidance for Space Vehicles	Koji OTSUBO	Jan. 1972
TR-259	Study on a Rotary-Drive Vibratory-Output Rate Gyro	Hiroshi YAMADA	Jan. 1972
TR-260	A High Sensitive Total Atmospheric Temperature Measuring Apparatus	Kenji NISHIO, Hiroyuki NOSE, Takeshi KOSHINUMA, Shigeo INOUE, Hiroshi USUI & Toshimi OHATA	Jan. 1972
TR-261	Strain Measurement of Solid Propellant Material with Birefringent Coating	Shinichi KOSHIDE	Jan. 1972
TR-262	A Structuctural Analysis of Cylinder-Cone-Cylinder Shells by F.E.M	Akinori OGAWA	Jan. 1972
TR-263	A Study of Subsonic, Two-Dimensional Wall-Interference Effects in a Perforated Wind Tunnel with Particular Reference to the NAL 2m×2m Transonic Wind Tunnel	Masao EBIHARA	Jan. 1972
TR-264	Flight Control System Design for Launch Vehicle with Liquid Propellant	Hidehiko MORI & Hajime KOSHIISHI	Jan. 1972
TR-265	Fluidic Turbine Inlet Gas Temperature Sensor	Kenji NISHIO, Seiki ENDO & Tokukazu ENDO	Jan. 1972
TR-266	Some Consideration on the Aerodynamic Characteristics for a Body of Rocket with Blunt Nose	Iwao KAWAMOTO	Jan. 1972

Development of Turbulent Boundary Layers Along the Curved Walls of an Annular Diffusing Passage[1]

Shoichi FUJII[2] and Theodore H. OKIISHI[3]

ABSTRACT

Turbulent boundary layer development along the curved walls of an axisymmetric diffusing annulus was determined experimentally and compared with results calculated using a form of the von Kármán momentum integral boundary layer equation and several sets of simple auxiliary equations. Based on the comparisons made, one iterative solution method for predicting curved wall annular diffuser boundary layer growth that yields fair results is proposed.

NOTATIONS

A Passage cross-section area

c Constant in radial equilibrium equation

c_f Local coefficient of friction, $\tau_0 \Big/ \frac{1}{2}\rho U_{p,\delta}^2$

c_p Local pressure coefficient, $(p-p_{in}) \Big/ \frac{1}{2}\rho U_{in}^2$

d Portion of the friction work performed in the boundary layer that is dissipated

$\bar{H}$ Energy thickness shape factor for flat plate flow, δ^{**}/θ

H Shape factor for flat plate flow, δ^*/θ

H_1 Shape factor for axisymmetric flow, δ_1^*/θ_1

$H_{\delta-\delta^*}$ Special shape factor, $(\delta-\delta^*)/\theta$

$\dot{m}$ Mass flow rate, $2\pi \int \rho V_z r dr$

P_{in} Static pressure at curved passage inlet

p Local static pressure

r Radial coordinate

r_0 Inner or outer casing radius

r_m Radius of curvature of meridional plane projection of a streamline

r_l Casing longitudinal radius of curvature

R_θ Reynolds number based on momentum thickness, $\frac{U\theta}{\nu}$

t Portion of the friction work performed in the boundary layer that becomes turbulent motion energy

U Free stream velocity for flat plate flow

U_{in} Free stream velocity at inlet to curved passage

U_p Potential flow velocity

$U_{p,\delta}$ Mean velocity at the interface of potential flow and boundary layer regions

u Mean local velocity within the boundary layer

$\bar{V}$ Average passage velocity, $\bar{V}=\frac{\dot{m}}{\rho A}$

V_z Axial velocity

x Coordinate along the casing or flat plate

y Coordinate normal to the casing or flat plate

z Parameter defined by Eq. (A-12)

Z Axial coordinate

β Angle between y and r

Γ Buri's shape factor, $\Gamma=\frac{\theta_1}{U_{p,\delta}}\frac{dU_{p,\delta}}{dx}\left(\frac{U_{p,\delta}\theta_1}{\nu}\right)^{1/4}$

δ Flat plate flow boundary layer thickness

δ_y Boundary layer thickness along a normal line

δ_r Boundary layer thickness along a radius

δ^{**} Flat-plate flow dissipation energy thickness, $\int_0^\delta \frac{u}{U}\left(1-\frac{u^2}{U^2}\right)dy$

δ^* Flat-plate flow displacement thickness, $\int_0^\delta \left(1-\frac{u}{U}\right)dy$

δ_1^* Axisymmetric flow displacement thickness, $\int_0^{\delta_y} \frac{r}{r_0}\left(1-\frac{u}{U_{p,\delta}}\right)dy$

---

1) Received February 14, 1972

2) Aero-Engines Division

3) Assistant Professor, Department of Mechanical Engineering and Engineering Research Institute, Iowa State University, Ames, Iowa, U.S.A.

δ_t^* Displacement thickness at the outer wall

δ_h^* Displacement thickness at the inner wall

θ Flat-plate flow momentum thickness, $\int_0^\delta \left(\frac{u}{U}\right)\left(1-\frac{u}{U}\right)dy$

θ_1 Axisymmetric flow momentum thickness, $\int_0^{\delta_y} \frac{r}{r_0}\left(1-\frac{u}{U_{p,\delta}}\right)\frac{u}{U_{p,\delta}}dy$

λ Streamline slope

ν Kinematic viscosity

ρ Fluid density

τ Fluid shearing stress

τ_0 Shear stress at the casing

INTRODUCTION

The turbulent boundary layer development along the walls of an internal flow passage is an important facet of turbomachinery design and analysis. For example, poor estimates of the boundary-layer thicknesses at an axial-flow compressor rotor inlet can result in significant incidence angle errors. Boundary layers also strongly influence turbomachine diffuser performance. Empirical "blockage" factors are used to determine the influence of wall bounary layers on the overall performance of turbomachine components with some success. These empirical blockage factors are, however, becoming less adequate as the demand for better designs increases. No entirely satisfactory general method of calculating the wall boundary layer development associated with the complicated flow through a turbomachine is currently available in the open literature. From an engineering point of view, the simplified but reliable methods of boundary layer calculation can be obtained with acceptable assumptions for special flow situations; for example, several attempts in this direction have already been made[1,2,3] for axial flow compressors. The authors are not aware of similar work related to flow through curved-wall annular diffusing passages. In this paper the von Kármán-momentum integral approach for boundary layer development calculation is used for predicting curved-wall annular diffuser boundary layer growth. Five different sets of auxiliary equations are evaluated by comparing experimental and calculated results. Based on this evaluation one iterative solution method for predicting curved-wall annular diffuser boundary layer growth is proposed. It is recognized that the effects of longitudinal (streamwise) and transverse (circumferential) curvature on the auxiliary equations can be significant as pointed out by Wilcken[4], Patel[5] and Cebeci[6]. As an initial step, however, it was felt that an assessment of how the most simple auxiliary equations—namely those inspired by flat plate flow—would do under the present circumstances would aid in further developing an adequate prediction technique.

ANALYTICAL PROCEDURE

A flow model consisting of developing annulus wall bounary layers which surround a potential flow core was adopted for the present calculations. The appropriate form of the von Kármán momentum integral equation[7] to be used is:

$$\frac{1}{r_0}\frac{d}{dx}(r_0\theta_1)+\frac{2+H_1}{U_{p,\delta}}\frac{dU_{p,\delta}}{dx}\theta_1 = \frac{c_f}{2}+\frac{\nu\sin^2\beta}{r_0 U_{p,\delta}^2}\int_0^{\delta_y}\frac{u}{r}dy \qquad (1)$$

where

$$\theta_1=\int_0^{\delta_y}\frac{r}{r_0}\left(1-\frac{u}{U_{p,\delta}}\right)\frac{u}{U_{p,\delta}}dy\,,$$

$$\delta_1^*=\int_0^{\delta_y}\frac{r}{r_0}\left(1-\frac{u}{U_{p,\delta}}\right)dy\,,$$

$$H_1=\delta_1^*/\theta_1\,.$$

This relationship assumes that several term involving turbulent velocity fluctuations will be accouted for by the auxiliary equations used and that longitudinal curvature is mild. The last term of the right hand side of equation (1) can be easily written as

$$\frac{\nu\sin^2\beta}{r_0^2 U_{p,\delta}}\left(\frac{2n+1}{n+1}\right)\theta_1$$

assuming that $u/U_{p,\delta}=(y/\delta_y)^n$. By considering the fact that the value of n ranged between 1/8 and 1/7 in our experimental data, $2n+1/n+1$ was approximated as 1.9 in the actual computation. If the function $U_{p,\delta}(x)$ is known either from experiment or from a potential flow portion solution, two other equations in addition to equation (1) are needed to determine the variation of θ_1, H_1, and c_f with x. Five different sets of auxiliary equations (see Appendix A) were selected from the literature and, together with them and the experimentally determined variation of $U_{p,\delta}(x)$, equation (1) was solved on a digital computer with the aid of the Runge-Kutta-Gill method[8]. Measured velocities near the edge of each boundary layer were connected by least-mean-squares curves of seventh order to provide the $U_{p,\delta}(x)$ input. This was done in order to evaluate the various sets of auxiliary equations. Based on this evaluation, appropriate auxiliary equations were combined with equation (1) and the variation of $U_{p,\delta}(x)$ obtained form a potential flow solution to form an iterative solution. The streamline curvature technique[9] was used to determine the potential flow field. The governing equations used were those expressing radial equilibrium,

$$V_z^2 = c^2 \exp \int \frac{2}{r_m \cos^3 \lambda} dr\,, \qquad (2)$$

and continuity,

$$\dot{m} = 2\pi \int \rho V_z r dr\,. \qquad (3)$$

In all instances values of displacement thickness, shape factor, and $U_{p,\delta}$ at the entrance of the curved passage were obtained experimentally.

EXPERIMENTAL PROCEDURE

Apparatus

The tests were conducted with a wooden annular diffuser [see Fig. 1 (a) for meridional plane

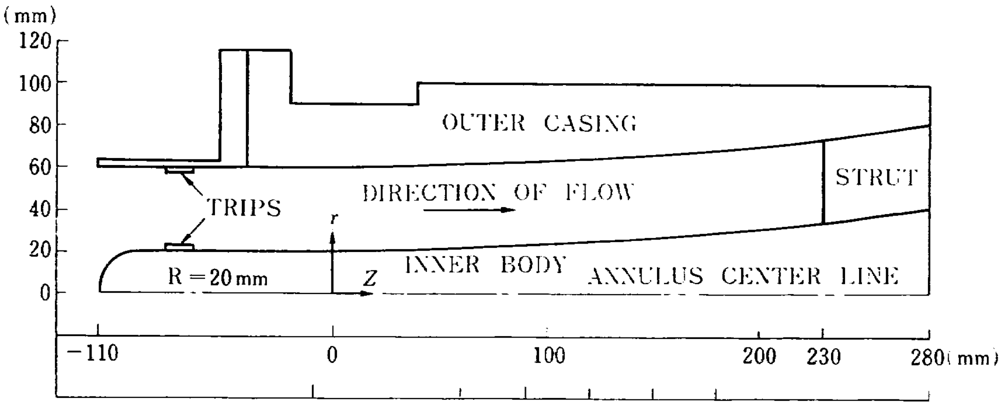

Fig. 1 (a). The diffusing passage.

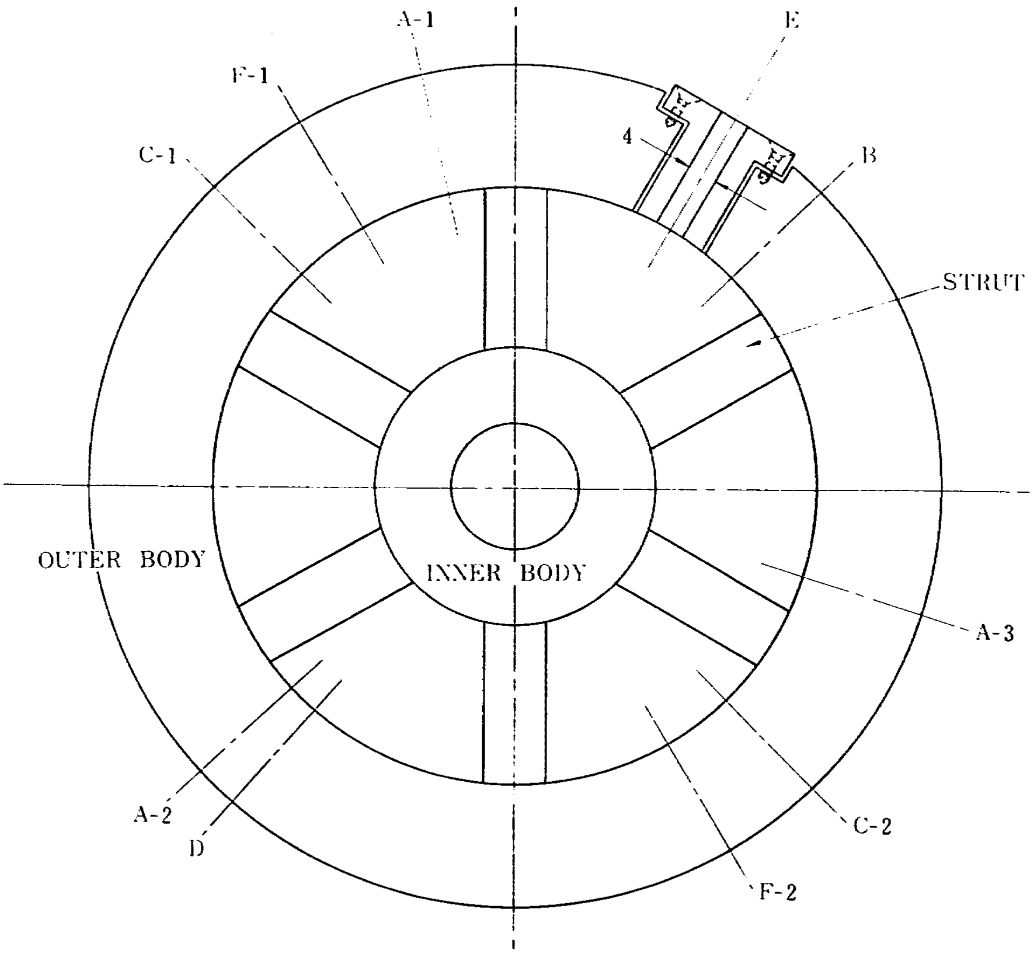

Fig. 1 (b). Circumferential spacing of inner body support and total-pressure probe access holes.

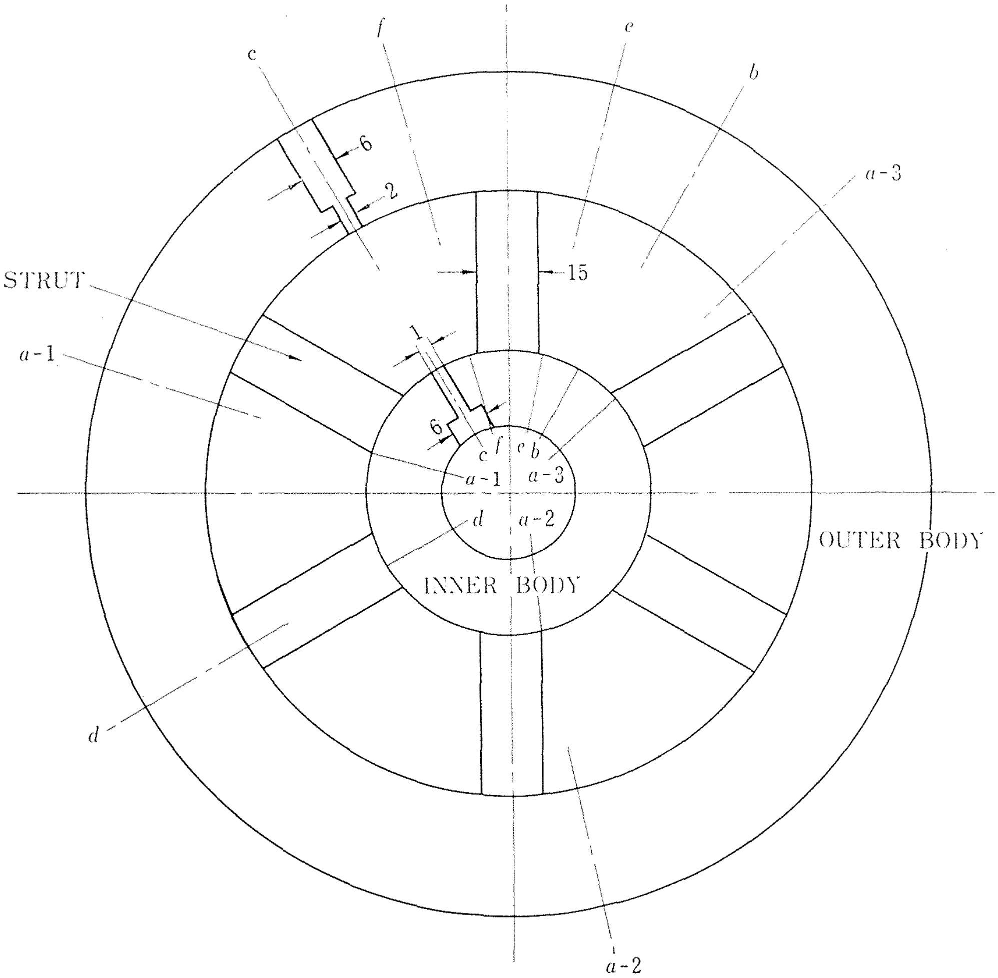

ALL LENGTHS IN MILLIMETERS

Fig. 1 (c). Circumferential spacing of inner body supports and static pressure taps.

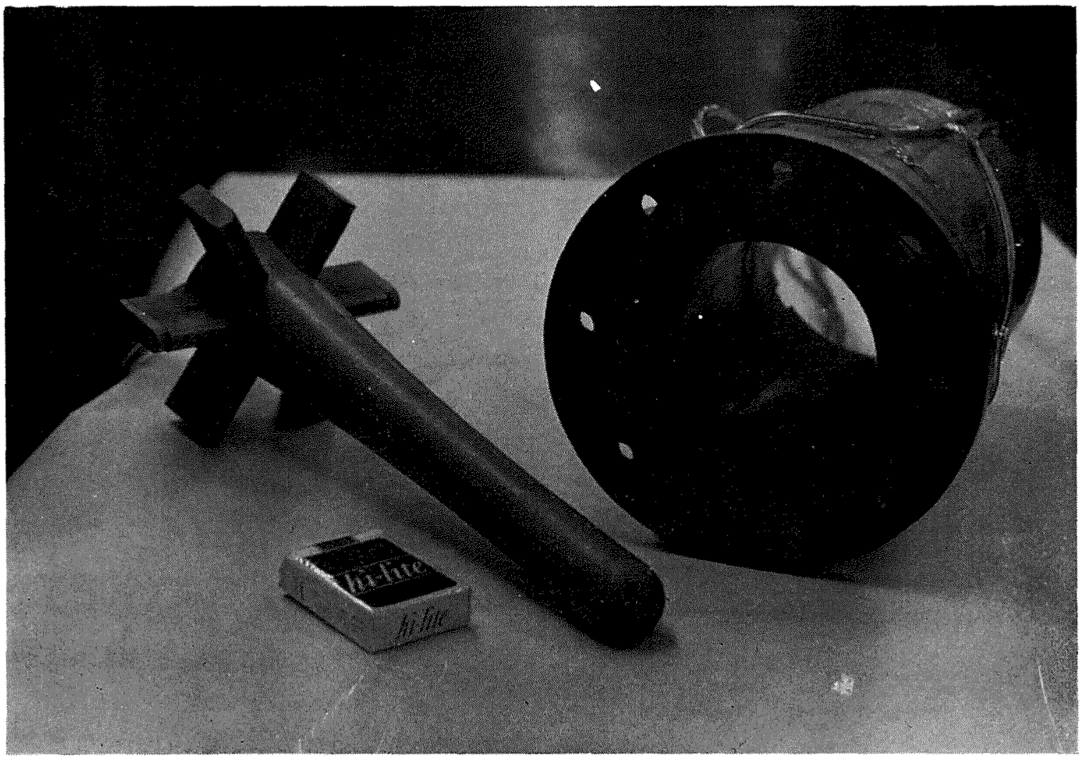

Fig. 2. Test section outer casing and center body.

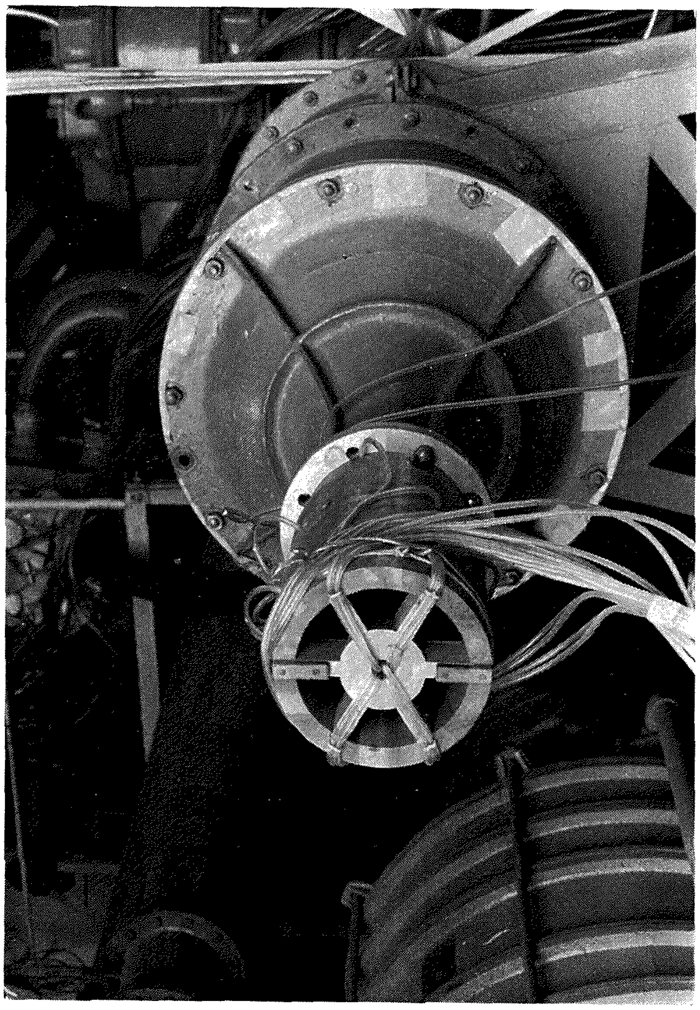

Fig. 3 (b). Test section mounted in place.

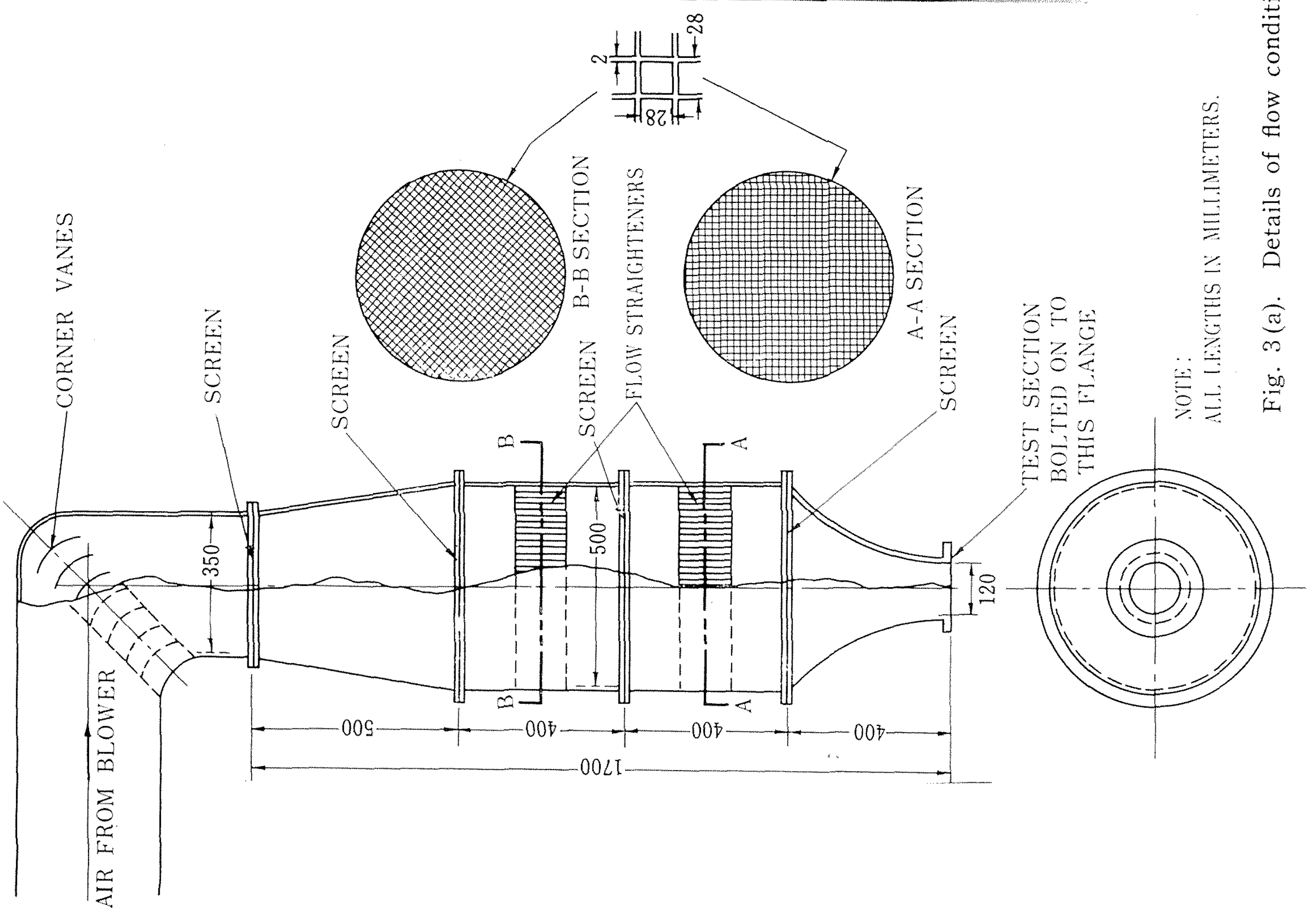

Fig. 3 (a). Details of flow conditioner upstream of the test section.

view]. The contours of the outer and inner walls were described by the parabolic curves,

$$r=0.00025Z^2+60 \text{ for the outer casing} \quad (4)$$
$$r=0.00025Z^2+20 \text{ for the inner casing}$$

and were designed to provide an adverse pressure gradient without flow separation. Buri's [see Schlichting[10)]] shape factor $\left[\Gamma=\frac{\theta_1}{U_{p,\delta}}\cdot\frac{dU_{p,\delta}}{dx}\left(\frac{U_{p,\delta}\theta_1}{\nu}\right)^{1/4}\right]$ was used as the separation criterion in the design step. The inner body was supported by six circumferentially spaced struts. Six measuring stations—A, B, C, D, E, and F—were available, the final measuring station F being located more than one strut chord length upstream from the strut leading edge. At station A three total-pressure-probe-survey access holes (A-1, A-2, and A-3) were drilled in the casing, with each hole spaced circumferentially 120 degrees apart. At each of the stations C and F two (C-1, C-2, F-1, and F-2) survey access holes spaced 180 degrees apart circumferentially were available for use. At each of the remaining stations only one survey access hole was available. The static pressures acting on inner and outer walls were measured with taps located in the hub and casing at these measuring stations. Circumferential uniformity of static pressure was examined only at station A. The static pressure measuring positions were labeled as a-1, a-2 and a-3 at station A, and b, c, d, and e at stations B, C, D, and E respectively. Figs. 1(b) and 1(c) indicate the relative circumferential positions of the struts, total-pressure survey access holes, and static pressure taps. Figure 2 shows the diffuser casing and hub. The two large holes near the leading edge of the hub, originally intended for use with supports, were sealed during the test runs.

A schematic diagram of the low-speed wind tunnel passage upstream of the annulus is shown in Fig. 3(a). Figure 3(b) shows the annulus mounted for testing. Airflow was provided by a centrifugal blower capable of producing a volume flow rate of 40 m³/min (1410 cfm) at 2920 rpm. Screens were placed at four sections of the inlet conduit in order to promote radial and circumferential uniformities of total impact. Two sets of 120 mm long straightners were installed in the inlet conduit to minimize swirl.

Dimentions of the total pressure probe are indicated in Fig. 4(a). The probes used had different angles between stem and impact tube axes to coincide with the annulus wall slopes at each measuring station. The probe support shown in

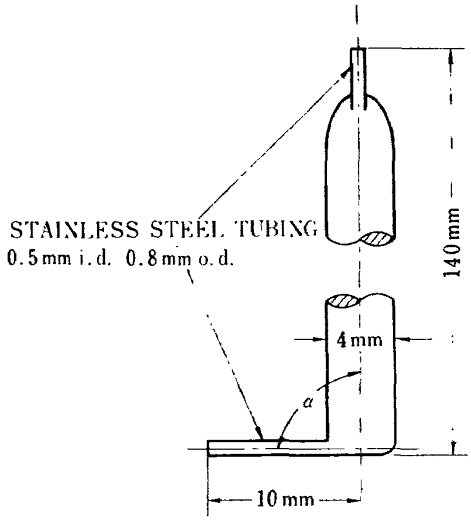

Fig. 4(a). Total-pressure probe.

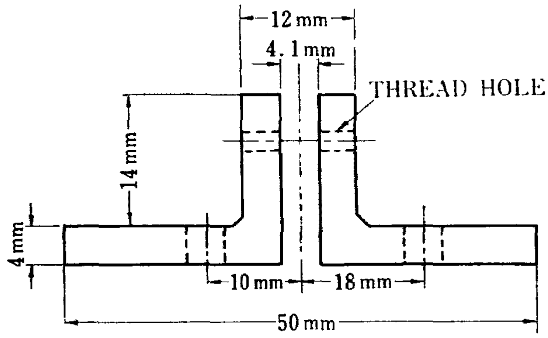

Fig. 4(b). Probe support.

Fig. 4(b) was attached to the diffuser casing and positioning of the probe was facilitated with calipers having a least count of 0.05 mm.

Measurements

Tests were conducted under three different flow conditions, namely, without boundary layer tripping, with 0.45 mm thick trips, and with 1.20 mm thick trips. The Reynolds number based on the momentum thickness ranged from about 0.5×10^3 at section A to 1.5×10^3 at section F for these tests. The inlet velocity was maintained at about 30 m/sec during all of the tests. The static pressure variation along each wall for the thick trip test is shown in Fig. 5.

Each test run consisted of a total-pressure survey traverse along a radius, static pressure readings, fluid and room temperature measurements, and atmospheric pressure readings with checks at the end of each run confirming that the test variables had not changed appreciably over the test period. The zero probe location was determined by contact between the probe and each wall surface. The radial traverses were made at intervals of 0.2 to 0.3 mm within the boundary layer and at intervals of 2.0 to 10.0 mm in the

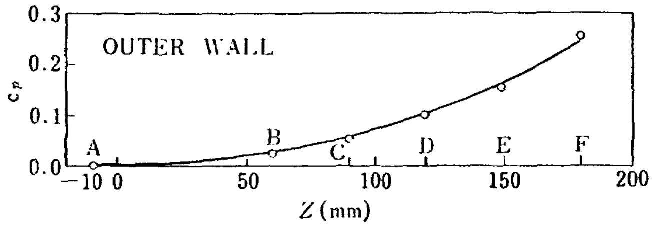

Fig. 5 (a). Wall static pressure variation along the outer casing of the test section.

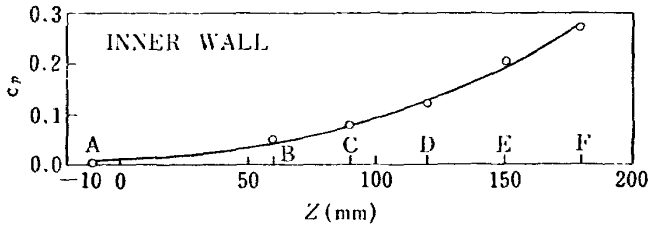

Fig. 5 (b). Wall static pressure variation along the inner casing of the test section.

potential flow core region. During a run, only one access hole was used at a time in order to avoid the problems associated with probe interference.

Reduction of Data

As mentioned previously, the total-pressure traverses were made along radii. The predicted boundary layer characteristics are associated with lines normal to the casing and hub surfaces. In this section, the method used for obtaining the "measured" normal-direction boundary layer characteristics is explained. Shown in Fig. 6 (a) is the radial traverse line of a measuring station. It extends from point G1 to G2. From G1 on the casing a normal line G1-G4 can be constructed. Similarly, line G2-G3 can be drawn through G2 on the hub. By assuming that the static pressure varied linearly from G1 to G2, we can calculate the velocity distribution along G1-G2 from the total pressure measurements associated with that line. By comparing this velocity distribution with the one obtained by the streamline curvature technique, assuming zero boundary layer thicknesses, we then can estimate the boundary layer thicknesses along G1-G2. These estimates did not change appreciably after further comparing the experimentally determined velocity profiles and those calculated with the streamline curvature technique and finite boundary layer thicknesses [see Fig. 6 (b)]. The corresponding thicknesses along G1-G4 and G2-G3 were then obtained with

$$\delta_y = \delta_r \cos\beta \,. \tag{5}$$

In order to obtain the integral thicknesses along G1-G4 and G2-G3, velocities along those lines were required. The static and total pressures leading to these velocities were obtained as follows. The static pressures at G3 and G4 were estimated from the static pressures measurements at G1 and G2 and elsewhere along the casing and hub. Passage static pressures were then assumed to vary linearly along the normal lines. The normal-line total pressures were estimated as being equal to those values measured on the radial line at $y/\cos\beta$ distance from the wall.

RESULTS AND CONCLUSIONS

As stated before, experimental data were gathered at three circumferentially spaced positions at station A and two circumferentially spaced

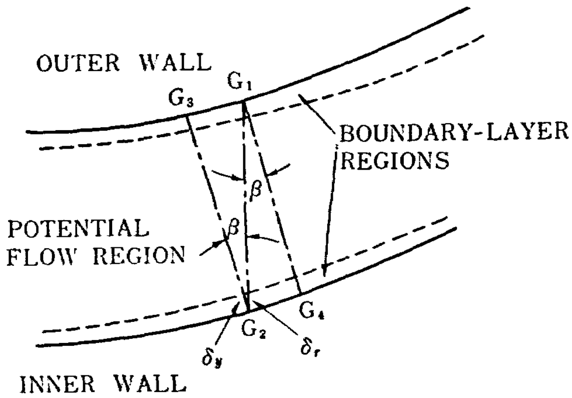

Fig. 6 (a). Relationship between the normal and radial coordinate directions.

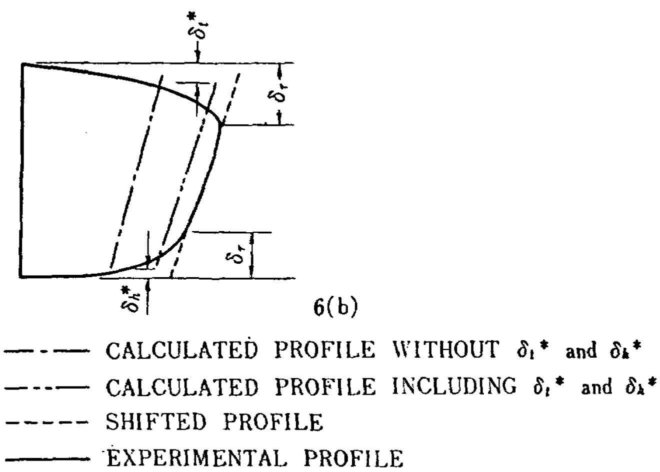

Fig. 6 (b). Approximation relationship between measured and calculated velocity profiles along a radius.

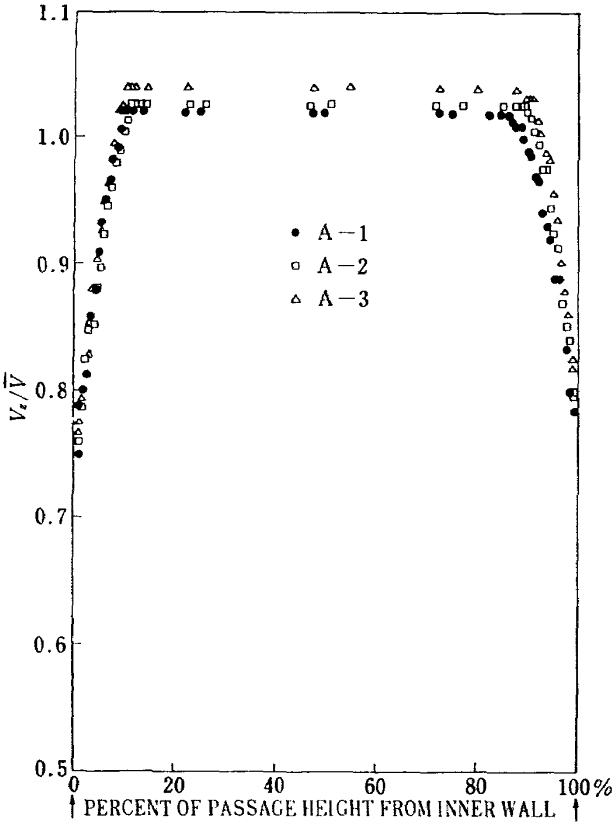

Fig. 7 (a). Velocity profiles (radial distribution) at measuring station A.

positions at stations C and F. These data for the thick trip case are shown in *Fig.* 7 and indicate that nearly axisymmetric behavior flow was maintained through the passage. Apparent mass flow rates through the channel were determined using the velocity distributions at every section. A scatter of about 5 to 6% was observed.

Figures 8 through 11 show the experimental data associated with the development of the boundary layers along the outer and inner walls of the annulus for the thick trip tests. Also shown are the computed values of displacement and momentum thicknesses and shape factor obtained using the five sets of auxiliary equations discussed in Appendix A, equation (1) and either the measured velocities at the edge of each boundary layer or the computed values obtained with an iterative solution. Since the thin trip and tripless cases exhibited nearly the same trends as the thick trip flow, only the data for the thick trip tests are shown.

A comparison between the values of δ_1^*, θ_1 and H_1 obtained experimentally with those determined by using the five different sets of auxiliary equations, equation (1), and experimentally determined $U_{p,\delta}(x)$ led to the conclusion that set 3 was supe-

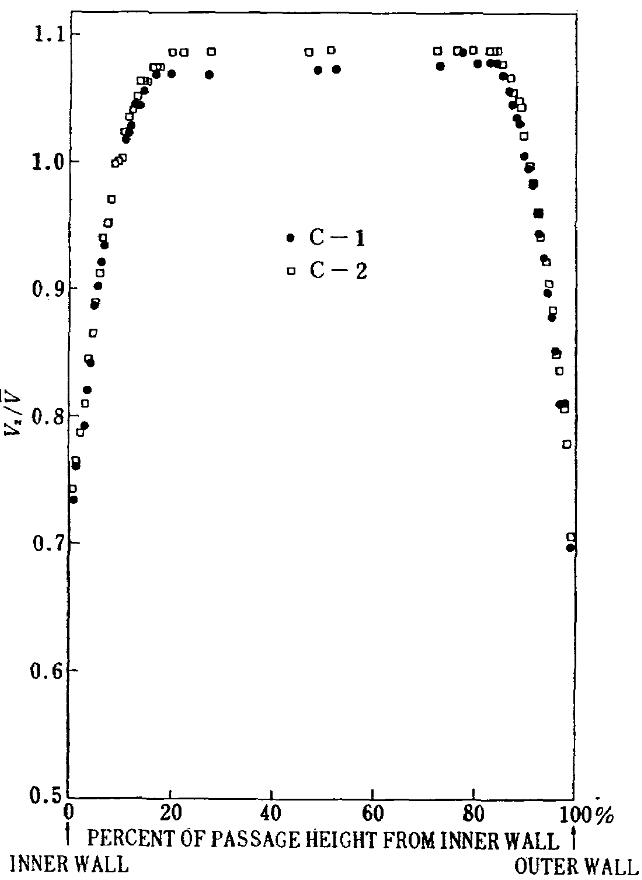

Fig. 7 (b). Velocity profiles (radial distribution) at measuring station C.

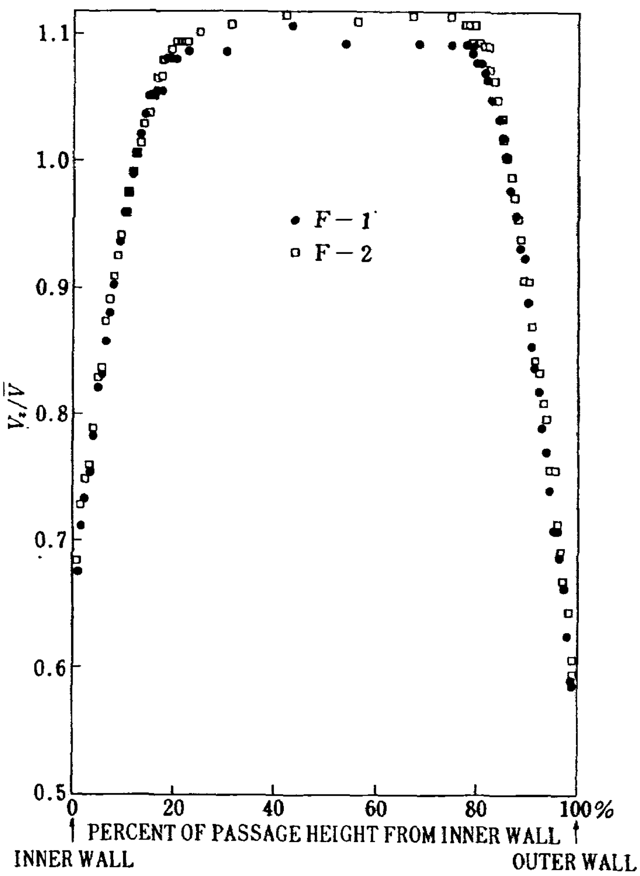

Fig. 7 (c). Velocity profiles (radial distribution) at measuring station F.

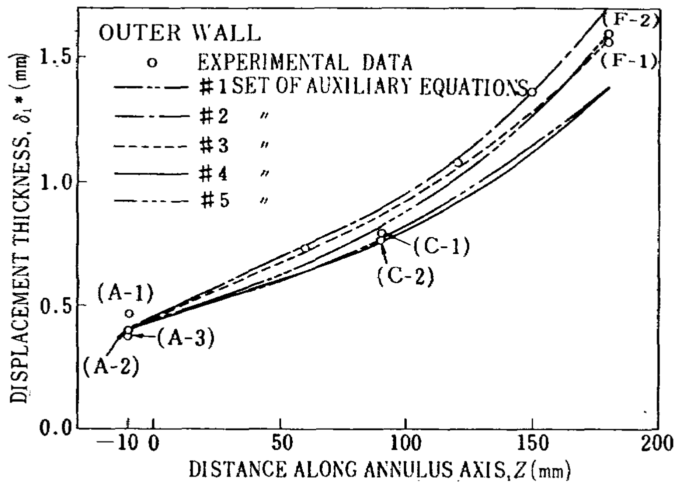

Fig. 8 (a). Comparison of measured and calculated (measured variation of $U_{p,\delta}(x)$ used as input) outer casing displacement thicknesses.

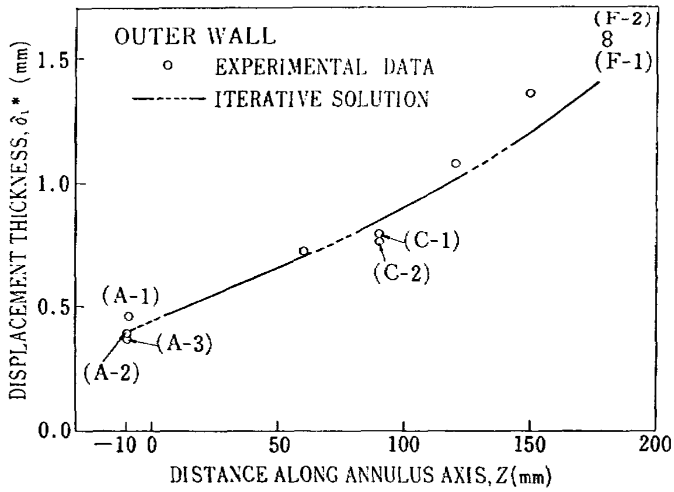

Fig. 9 (a). Comparison of measured and calculated (iterative solution) outer casing displacement thicknesses.

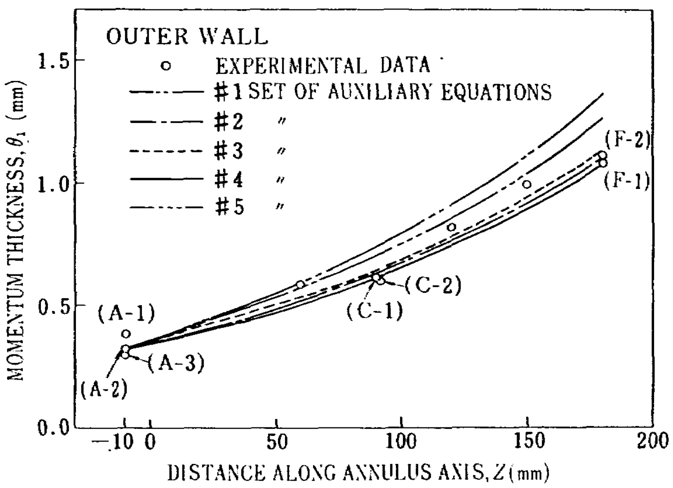

Fig. 8 (b). Comparison of measured and calculated (measured variation of $U_{p,\delta}(x)$ used as input) outer casing momentum thicknesses.

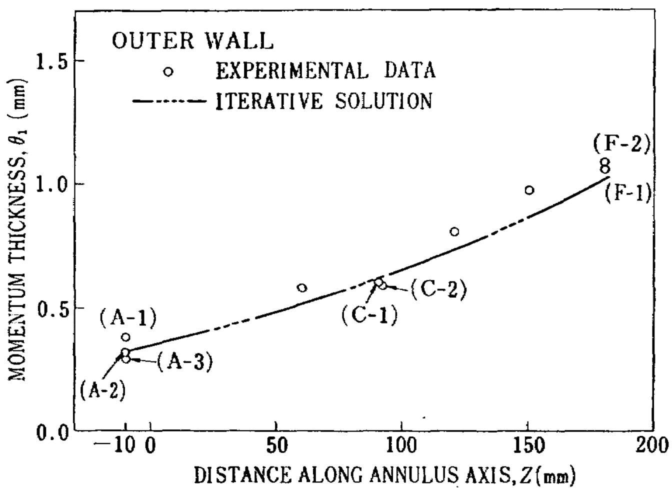

Fig. 9 (b). Comparison of measured and calculated (iterative solution) outer casing momentum thicknesses.

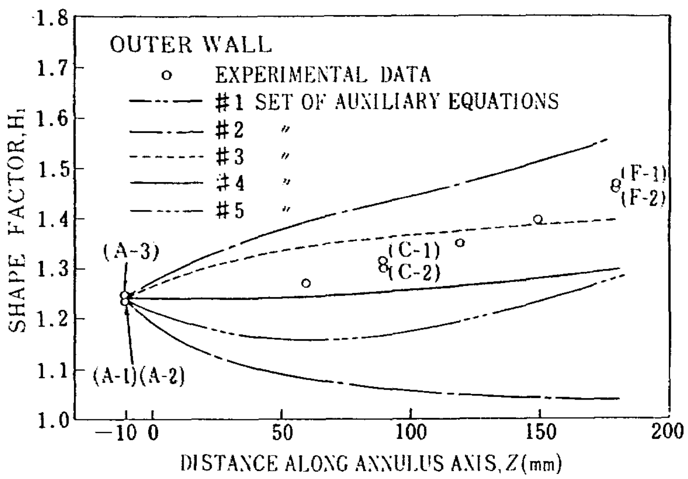

Fig. 8 (c). Comparison of measured and calculated (measured variation of $U_{p,\delta}(x)$ used as input) outer casing shape factors.

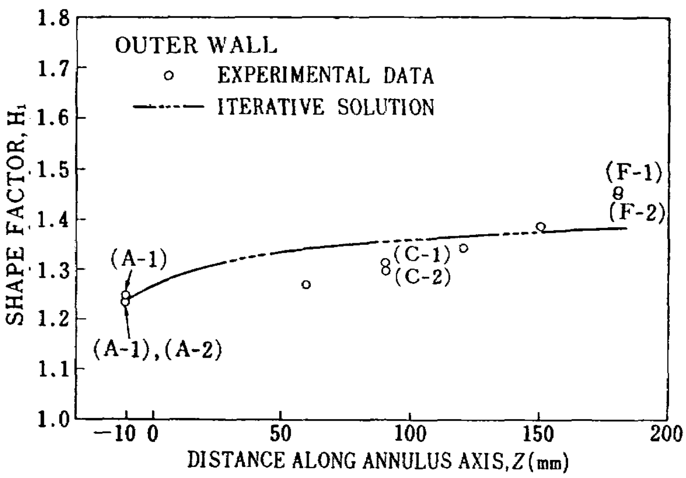

Fig. 9 (c). Comparison of measured and calculated (iterative solution) outer casing shape factors.

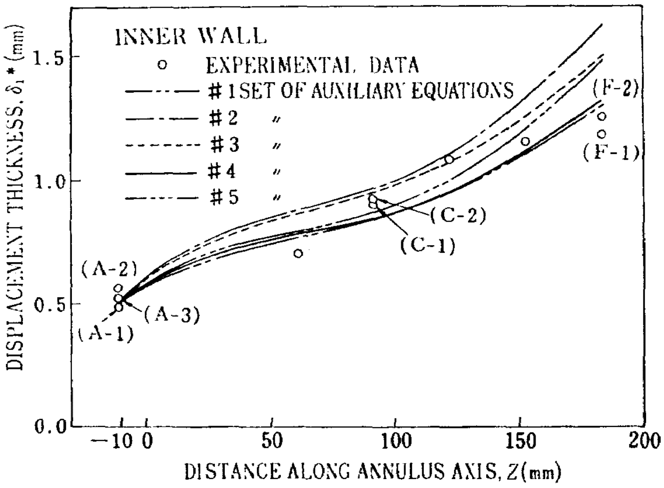

Fig. 10 (a). Comparison of measured and calculated (measured variation of $U_{p,\delta}(x)$ used as input) inner casing displacement thicknesses.

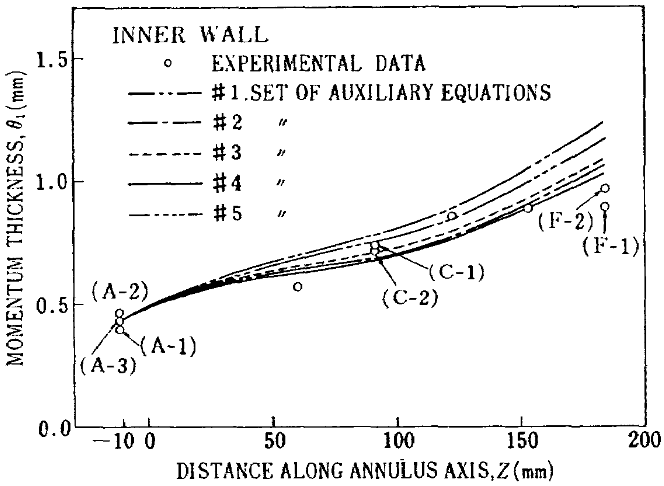

Fig. 10 (b). Comparison of measured and calculated (measured variation of $U_{p,\delta}(x)$ used as input) inner casing momentum thicknesses.

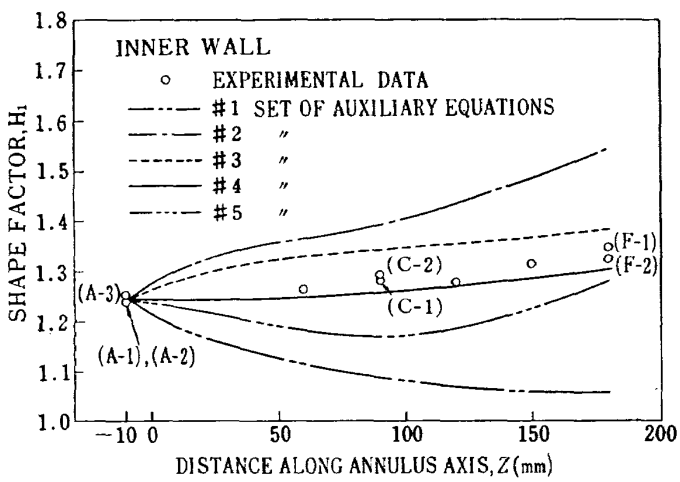

Fig. 10 (c). Comparison of measured and calculated (measured variation of $U_{p,\delta}(x)$ used as input) inner casing shape factors.

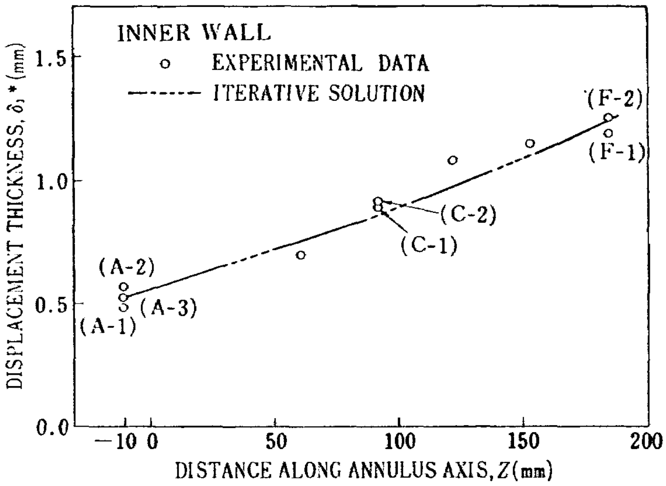

Fig. 11 (a). Comparison of measured and calculated (iterative solution) inner casing displacement thicknesses.

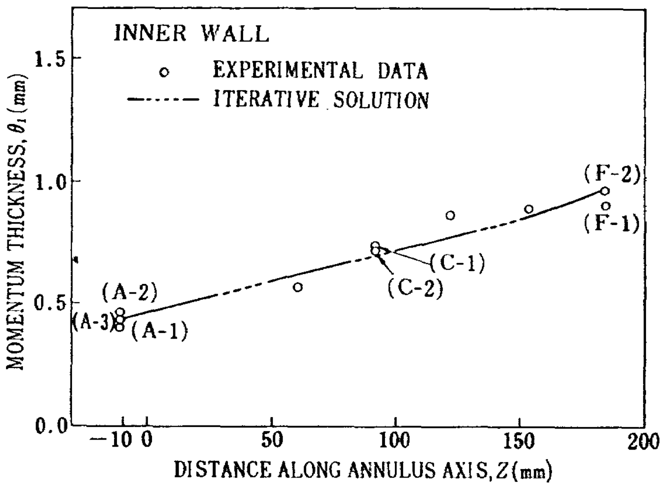

Fig. 11 (b). Comparison of measured and calculated (iterative solution) inner casing momentum thicknesses.

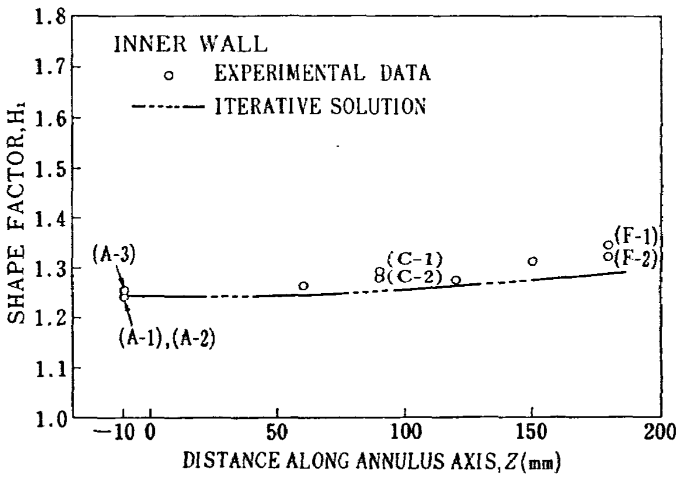

Fig. 11 (c). Comparison of measured and calculated (iterative solution) inner casing shape factors.

Table 1. Ratio of the radii of longitudinal and transverse curvatures to the boundary layer thickness.

Section	r_l/δ_r		r_0/δ_r	
	Outer wall	Inner wall	Outer wall	Inner wall
A	∞	∞	13.3	4.4
B	445.0	445.0	9.4	3.8
C	313.5	364.8	10.9	3.1
D	352.8	287.3	7.8	3.2
E	246.0	269.0	8.0	3.4
F	246.0	289.2	8.0	4.0

rior to the rest for predicting outer wall development while set 4 was best for the inner wall. This observation led to the execution of an iterative solution involving auxiliary equations set 3 for the outer wall, auxiliary equations set 4 for the inner wall, equation (1), and the streamline curvature equations [equations (2) and (3)]. The results of this analytical solution appear to be fair considering the approximations made. Table 1 indicates the passage longitudinal and transverse curvatures. Bradshaw[11] suggests that longitudinal curvature associated with a value of $r_l/\delta<300$ is significant. Cebeci[6] states that when the radius of a body in a viscous flow is of the same order of magnitude as the thickness of the boundary layer, the transverse curvature effect on skin friction becomes appreciable. Further improvements in the present calculation method will probably be obtained when the auxiliary equations are revised to clearly reflect curvature effects. Research along this line is in progress.

APPENDIX A

Shown below are several sets of auxiliary equations based on flat-plate boundary layer flow. These auxiliary equations are assumed to apply, without modification, for the axisymmetric flow case at hand.

Set 1

The moment-of-momentum boundary-layer equation for a power-law velocity profile[12] is:

$$\theta\frac{dH}{dx}=-\frac{H(H+1)(H^2-1)}{2}\frac{\theta}{U}\frac{dU}{dx}+(H^2-1)H\frac{c_f}{2}-(H+1)(H^2-1)\times\int_0^\delta\frac{\tau}{\rho U^2}\frac{dy}{\delta}\,. \qquad \text{(A-1)}$$

For a uniform shear stress distribution in the boundary layer,

$$\int_0^\delta\frac{\tau}{\rho U^2}\frac{dy}{\delta}=\frac{c_f}{2}$$

and equation (A-1) becomes

$$\theta\frac{dH}{dx}=-\frac{H(H+1)(H^2-1)}{2}\frac{\theta}{U}\frac{dU}{dx}-(H^2-1)\frac{c_f}{2}\,. \qquad \text{(A-2)}$$

The skin-friction coefficient can be approximated by the familiar Ludwieg-Tillman[13] equation:

$$c_f=(0.246)(10^{-0.678H})(R_\theta^{-0.268})\,. \qquad \text{(A-3)}$$

Equations (A-2) and (A-3) then are auxiliary equations which together with equation (1) and $U_{p,s}(x)$ can be solved numerically.

Set 2

If instead of a uniform shear distribution, the one for zero-pressure gradient boundary layer flow is assumed along with a power law velocity profile, the shear stress integral of equation (A-1) becomes[14]:

$$\int_0^\delta\frac{\tau}{\rho U^2}\frac{dy}{\delta}=\frac{0.06(H-1)}{(H+1)(H+3)}R_\theta^{-0.10}$$

and equation (A-1) reduces to:

$$\theta\frac{dH}{dx}=-\frac{H(H+1)(H^2-1)}{2}\frac{\theta}{U}\frac{dU}{dx}+(H^2-1)(H)\frac{c_f}{2}-0.06\frac{(H^2-1)(H-1)}{(H+3)}R_\theta^{-0.10}\,. \qquad \text{(A-4)}$$

Equations (A-4) and (A-3) form the auxiliary set.

Set 3

If the energy integral equation is combined with the momentum integral equation the result[15] is:

$$\theta\frac{d\bar{H}}{dx}=(H-1)\bar{H}\frac{\theta}{U}\frac{dU}{dx}+2\frac{d+t}{\rho U^3}-\bar{H}\frac{c_f}{2} \qquad \text{(A-5)}$$

where

$$\frac{d+t}{\rho U^3}=\int_0^\delta\frac{\tau}{\rho U^2}\frac{\partial}{\partial y}\left(\frac{u}{U}\right)dy$$

represents the dimensionless friction work performed in the boundary layer by the shearing stress τ. The amount d is the portion dissipated, while t is the energy of turbulent motion. Truckenbrodt[15] suggests that $t\ll d$ and proposes an empirical relationship for d, namely,

$$\frac{d}{\rho U^3}=\frac{0.0056}{(U\theta/\nu)^{1/6}}\,.$$

This result, combined with equation (A-5), yields:

$$\theta\frac{d\bar{H}}{dx}=\bar{H}\left[(H-1)\frac{\theta}{U}\frac{dU}{dx}-\frac{c_f}{2}\right]+0.0112R_\theta^{-1/6}. \qquad \text{(A-6)}$$

For a logarithmic boundary-layer velocity profile family, the relationship between $\bar{H}$ and H is given approximately by[14]:

$$\bar{H}=\frac{1.02+0.87H+0.095H^2}{H}. \qquad \text{(A-7)}$$

Equations (A-7), (A-6), and (A-3) form auxiliary equation set 3.

Set 4

An empirical relationship for shape factor development proposed by von Doenhoff and Tetervin[16] is:

$$\theta\frac{dH}{dx}=e^{4.680(H-2.975)}\left[-\frac{\theta}{U}\frac{dU}{dx}\frac{4}{c_f}-2.035(H-1.286)\right] \qquad \text{(A-8)}$$

where c_f is obtained by the Squire and Young[17] formula:

$$\frac{c_f}{2}=\frac{0.0288}{[\log_{10}(4.075(U\theta/\nu))]^2}. \qquad \text{(A-9)}$$

Equation (A-9) and (A-8) form auxiliary equation set 4.

Set 5

The boundary layer entrainment equation[18] is:

$$\frac{1}{U}\frac{d}{dx}[(U)(\delta-\delta^*)]=F(H_{\delta-\delta^*}) \qquad \text{(A-10)}$$

where $H_{\delta-\delta^*}$ is a special shape factor defined by:

$$H_{\delta-\delta^*}\equiv\frac{\delta-\delta^*}{\theta}=G(H). \qquad \text{(A-11)}$$

If z is defined by

$$z\equiv\theta[G(H)], \qquad \text{(A-12)}$$

then

$$\frac{dz}{dx}=\frac{d\theta}{dx}G(H)+\theta\frac{dG(H)}{dH}\frac{dH}{dx}. \qquad \text{(A-13)}$$

Equation (A-10), (A-11) and (A-12) combine to form:

$$\frac{dz}{dx}=F[G(H)]-\frac{1}{U}\frac{dU}{dx}z. \qquad \text{(A-14)}$$

Equation (A-14), (A-13) and (A-3) form auxiliary equation set 5.

ACKNOWLEDGEMENTS

The authors are grateful to the Aero-Engines Division of the National Aerospace Laboratory, Tokyo, Japan and the Engineering Research Institute of Iowa State University, Ames, Iowa for their support of the work leading to this report. Messrs. H. Nishiwaki and M. Gomi of the National Aerospace Laboratory deserve special recognition for their cooperation in obtaining the experimental and calculated results reported. The senior author is appreciative of the fellowship extended him while a Research Associate at Iowa State University by Professors G. K. Serovy and P. Kavanagh and Mr. Max Miller, all of Iowa State University.

REFERENCES

1) Jansen, W., "The Application of End-Wall Boundary-Layer Effects in the Performance Analysis of Axial Compressors," ASME Paper 67-WA/GT-11, 1967.
2) Stratford, B. S., "The Use of Boundary Layer Techniques to Calculate the Blockage From the Annulus Boundary Layer in a Compressor," ASME Paper 67-WA/GT-7, 1967.
3) Mellor, G. L. and Wood, G. M., "An Axial Compressor End-Wall Boundary Layer Theory," ASME Paper 70-GT-80, 1970.
4) Wilcken, H., "Effect of Curved Surfaces on Turbulent Boundary Layers," U.S. NASA TT-F-11,421, 1967.
5) Patel, V. C., "Effects of Curvature on the Turbulent Boundary Layer," Great Britain Aeronautics Research Council 30427, 1968.
6) Cebeci, T., "Laminar and Turbulent Incompressible Boundary Layers on Slender Bodies of Revolution in Axial Flow," ASMF Trans., Journal of Basic Engineering, September 1970.
7) Rouse, H., *Advanced Mechanics of Fluids*, John Wiley and Sons, New York, 1958.
8) Moriguchi, S., *Introduction to FORTRAN IV*, Tokyo University Press, Tokyo, Japan, 1961.
9) Fujii, S. and Uno, T., "Streamline-Curvature Approach to Duct-Flow Problems," Japan National Aerospace Laboratory, TR-140, 1967.
10) Schlichting, H., *Boundary Layer Theory*, McGraw-Hill Book Co., Inc., New York, 1960.
11) Bradshaw, P., "The Analogy Between Stremline Curvature and Buoyacy in Turbulent Shear Flow," Journal of Fluid Mechanics, March 27, 1969.
12) Tetervin, N. and Lin, C. C., "A General Integral Form of the Boundary-Layer Equation for Incompressible Fow with an Application to the Calculation of the Separation Point of Turbulent Boundary Layers," U.S. NACA Report 1046, 1951.
13) Ludwieg, H. and Tillmann, W., "Investiga-

tion of the Wall-Shearing Stress in Turbulent Boundary Layers," U.S. NACA TM 1285, 1950.

14) Moses, H. L. and Chappell, J. R., "Turbulent Boundary Layers in Diffusers Exhibiting Partial Stall," ASME Trans., Journal of Basic Engineering, September 1967.

15) Truckenbrodt, E., "A Method of Quadrature for Calculation of the Laminar and Turbulent Boundary Layer in Case of Plane and Rotationally Symmetrical Fow," U.S. NACA TM 1379, 1955.

16) von Doenhoff, A. E. and Tetervin, N., "Determination of General Relations for the Behavior of Turbulent Boundary Layer, "U.S. NACA Report 772, 1943.

17) Squire, H. B. and Young, A. D., "The Calculation of Profile Drag of Airfoils," Great Britain Aeronautical Research Council *R* and *M* 1838, 1937.

18) Head, M. R., "Entrainment in the Turbulent Boundary Layer," Great Britain Aeronautical Research Council *R* and *M* 3152, 1958.

19) Fujii, S. and Okiishi, T. H., "Curved Diffusing Annulus Turbulent Boundary-Layer Development," Journal of Aircraft, Vol. 9, No. 2, February 1972, pp. 97-98.

TECHNICAL REPORT OF NATIONAL AEROSPACE RABORATORY
TR-278T

航空宇宙技術研究所報告 278 T 号(欧文)

昭和 47 年 2 月 発行

発行所 航空宇宙技術研究所
東京都調布市深大寺町 1,880
電話武蔵野三鷹(0422)47-5911(大代表)

印刷所 有限会社 啓文堂松本印刷
東京都文京区水道 2—7—5

Published by
NATIONAL AEROSPACE LABORATORY
1,880 Jindaiji, Chōfu, Tokyo
JAPAN

Printed in Japan